Frame Design Using Nonprismatic Members – Satisfying the Need for Speed

Bálint Vaszilievits-Sömjén[1], József Szalai[2], Donald W. White[3]

Abstract

This paper discusses a combination of best practices and procedures from recent work in Europe and the US, providing rational and economical calculations addressing the complexities associated with frame design using nonprismatic members. Recommendations are provided in the context of US design practice. A primary objective is to achieve maximum simplicity, transparency, and design speed while facilitating rigor of the underlying calculations. The paper provides several focused examples illustrating the recommended design verification procedures.
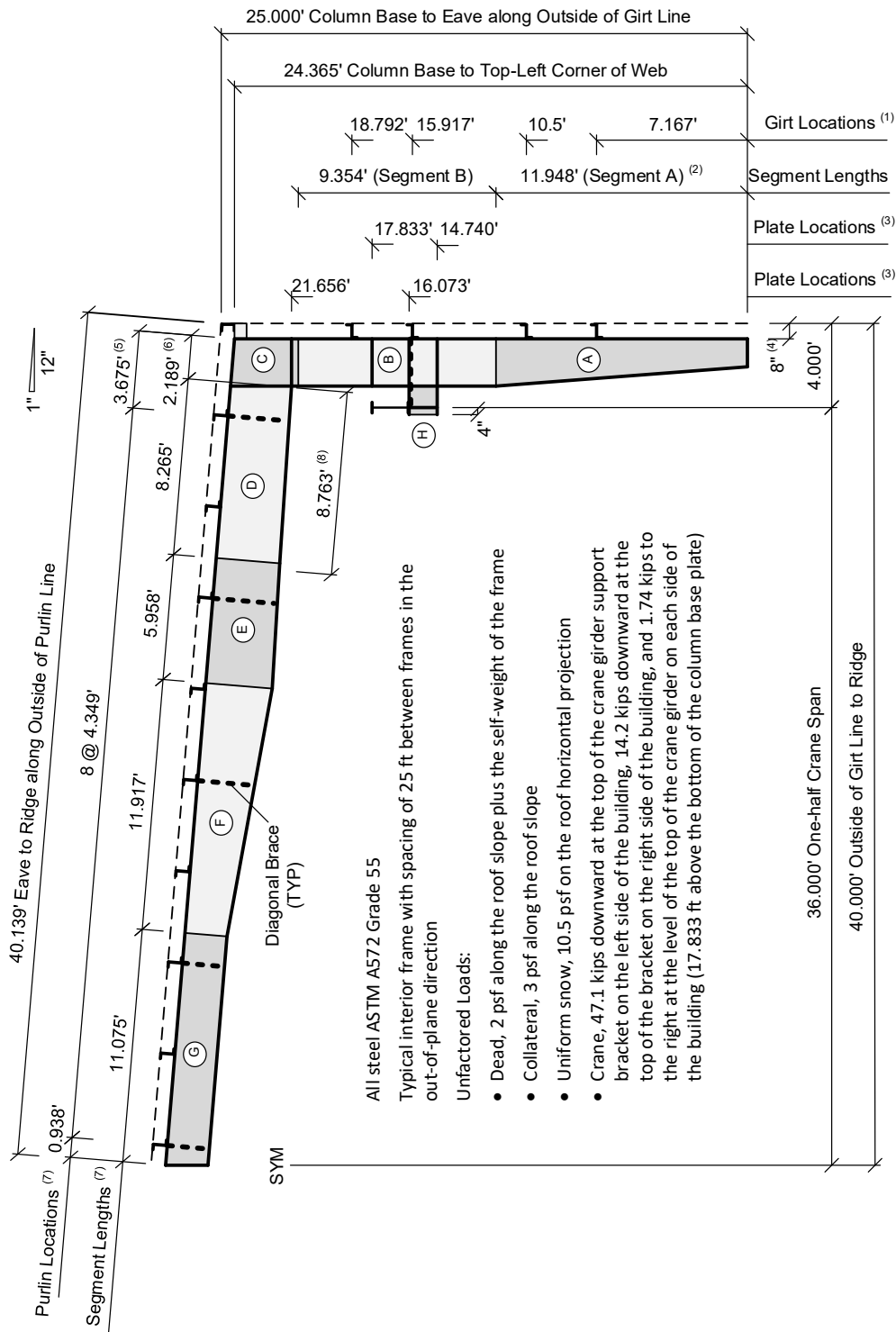
1. Introduction

There are numerous situations in structural engineering practice where frames are designed as planar structures, braced in the out-of-plane direction, and subjected to loads only within the plane of the frame. Metal building frames are a common subset of these types of designs. Figure 1, from the AISC/MBMA Design Guide 25 (White et al. 2021) (referred to as DG25 in this paper), is one example of such a frame. Out-of-plane buckling limit states often govern the strength of these structures. These types of frames commonly employ web taper, and steps in the web thicknesses and flange widths and thicknesses, to achieve the greatest design economy. Specific frame member cross-sections may be singly symmetric, and the arrangements of the out-of-plane bracing can be relatively complex. For example, the inside flanges of the members are often braced at fewer locations than the outside flanges, and the bracing configuration can be relatively general around the knee joints. The stability limit states are influenced by the geometry, the joint details, and the arrangement of the out-of-plane bracing at the various positions within the frame.

Researchers and practicing engineers have made significant progress advancing design methods for nonprismatic members and frames composed of such members. In the US, many of these advances have been captured in DG25. In addition, recent research (Slein et al. 2022 and 2023; Phillips et al. 2023a and b) has quantified built-up I-section member resistances substantially larger than present AISC 360 (AISC 2022) and Eurocode 3 (CEN 2005) predictions while also demonstrating substantial over-prediction by the AISC 360 provisions in some instances. Furthermore, Eurocode 3 Part 1-1 Section 6.3.4 provides a General Method addressing the out-of-plane buckling strength of structural components (Szalai 2011a and b; Szalai and Papp 2011).

---

[1] Senior Research Engineer, Consteel Solutions Ltd, Hungary <balint.vaszilievits@consteelsoftware.com>, PhD Student, Széchenyi István Egyetem, Győr, Hungary

[2] PhD, Senior Research Engineer, Managing Director, Consteel Solutions Ltd, Hungary <jozsef.szalai@consteelsoftware.com>

[3] Professor, Structural Engineering, Mechanics and Materials, Georgia Institute of Technology, USA < dwhite@ce.gatech.edu>

25.000' Column Base to Eave along Outside of Girt Line

24.365' Column Base to Top-Left Corner of Web

18.792' 15.917'   10.5'   7.167'   Girt Locations [1]

9.354' (Segment B)   11.948' (Segment A) [2]   Segment Lengths

17.833' 14.740'   Plate Locations [3]

                                                 Plate Locations [3]

21.656'   16.073'

1"
12"

3.675' [5]
2.189' [6]

C   B   A

8" [4]
4.000'

H

4"

8.265'

8.763' [8]

D

5.958'

E

11.917'

F

11.075'

G

40.139' Eave to Ridge along Outside of Purlin Line

8 @ 4.349'

0.938'

Purlin Locations [7]

Segment Lengths [7]

SYM

Diagonal Brace (TYP)

All steel ASTM A572 Grade 55

Typical interior frame with spacing of 25 ft between frames in the out-of-plane direction

Unfactored Loads:
- Dead, 2 psf along the roof slope plus the self-weight of the frame
- Collateral, 3 psf along the roof slope
- Uniform snow, 10.5 psf on the roof horizontal projection
- Crane, 47.1 kips downward at the top of the crane girder support bracket on the left side of the building, 14.2 kips downward at the top of the bracket on the right side of the building, and 1.74 kips to the right at the level of the top of the crane girder on each side of the building (17.833 ft above the bottom of the column base plate)

36.000' One-half Crane Span

40.000' Outside of Girt Line to Ridge

Footnotes:
[1] The girt locations are measured from the bottom of the column base plate to the bottom of the corresponding clip.
[2] The length of segment A is measured from the bottom of the column base plate.
[3] The plate locations are measured from the bottom of the column base plate to the bottom of the plate.
[4] The outset girts and purlins are 8 in. deep. The corresponding distance to the outside edge of the column web is 8.75 in.
[5] The first purlin location is measured from the top-left corner of the column web to the left side of the corresponding clip.
[6] The start of segment D is taken as the position along the top edge of the web at the roof girder cross section (perpendicular to the design axis) corresponding to the intersection of the bottom edge of the web with the right-hand face of the roof girder connection plates.
[7] The purlin locations and segment lengths are measured on-slope along the top edge of the roof girder web.
[8] The 8.763 ft length is the location of a transition in the bottom flange from segment D to segment E, measured from the start of segment D on-slope along the top edge of the roof girder web.

Figure 1: Geometry, material, and loads for example clear-span crane-building frame, adapted from the AISC/MBMA DG25 (White et al. 2021)

Both the General Method and the DG25 approaches take advantage of 14-dof frame finite element capabilities, based on thin-walled open-section beam theory, to determine rigorous elastic eigen-value buckling results. The respective design solutions can address all of the above-listed member and frame characteristics.

The design procedures recommended in this paper are a specific subset of the methods discussed in DG25 but with several advancements maximizing the simplicity, transparency, accuracy, and speed of the calculations:

1) The in-plane structural analysis is conducted employing specific Direct Analysis Method (DM) rules described in DG25, considering geometric imperfections within the plane of the structure as appropriate. The recommended approach dramatically simplifies the handling of the in-plane stability limit states.
2) The member strength verifications focus on cross-section strength-to-demand ratios to identify critical cross-sections where the subsequent calculations should be performed. This is a feature of the Eurocode 3 General Method, and this approach is recommended to reduce the number of member strength verifications that need be considered in the DG25 procedures.
3) In addition, the member strength verifications utilize elastic buckling load-to-demand ratios. These ratios may be calculated to assess separate axial loading and flexure alone. However, the Eurocode 3 General Method specifies the calculation of member elastic buckling load-to-demand ratios under the actual combined axial and flexural loading.

2. The General Method Concept
The traditional way of designing members subjected to combined axial compression and bending simplifies the calculations by separating the different load effects. The strength limit states and the associated design equations for pure axial compression and flexure are defined independently. At the end of the verification process, a simple interaction equation connects the governing strength values for the pure cases.

The above simplifications are partly due to limitations of calculation tools for handling combined loading. In addition, for simple cases, it is easier to understand and calculate member strengths under the pure load effects. Closed-form analytical solutions exist for the elastic buckling strength of prismatic members having simple bracing and end conditions, subjected separately to pure axial compression and bending. Accordingly, the axial compressive strength associated with flexural, torsional, flexural-torsional, or constrained-axis buckling is calculated independently from the flexural strength due to LTB. However, the above analytical solutions are, at best, coarse approximations of the true strengths for members having general bracing arrangements (e.g., different and unequal brace spacing on each flange) and general end conditions. Furthermore, the closed-form equations offer only coarse approximations of the strengths for members having steps and/or tapers in the cross-section geometry along their lengths.

Recently, however, the everyday use of software has opened new possibilities for evaluating the influence of complex parameters in the design for structural stability. Software solutions for elastic linear buckling analysis (ELBA) are particularly robust and promising. Moreover, these analysis capabilities are becoming more and more available in professional design software. As such, they can be used efficiently to calculate elastic critical buckling loads or stresses, replacing more limited analytical formulae. Furthermore, the use of ELBA with high-level numerical FE models (satisfying the requirements described in Section 8) can:

- Eliminate the need to focus solely on the separate pure load effects, and
- Solve cases outside the limits of standard analytical formulae, e.g., nonprismatic (tapered, haunched, and stepped) members, irregular bracing conditions, general end conditions, etc.

Nevertheless, these higher-level analysis possibilities are incompatible with current design standards in cases where the standards are based on the separation into pure load effects and require these separate solutions accordingly. The General Method addresses this situation. Eurocode 3 has incorporated the General Method in its provisions for more than 20 years. However, the General Method concept can be applied with any design standard. ***The basic idea of the General Method is that the complex member buckling modes – involving the interaction of the flexural, torsional-flexural, and lateral-torsional buckling under combined axial compression and flexure – are calculated as a single out-of-plane buckling limit state.*** To connect the above capabilities with codified member strength calculations, the General Method uses a single (out-of-plane) member slenderness parameter λ_{op}, determined from the elastic buckling load, as a fundamental dependent variable for the final out-of-plane buckling strength verifications. The parameter λ_{op} replaces the slenderness parameter associated with the separate pure loading limit states (or the effective unbraced length) for flexural, torsional-flexural, or lateral-torsional buckling. The designer employs λ_{op} in the ordinary equations of the design standard for the axial compressive and flexural strengths, ensuring conformity with the standard. The General Method is a natural way of handling the interaction between the axial compression and bending effects and the corresponding stability-related member strengths. This method was based initially on a heuristic formulation verified by experimental results (Bijlaard et al. 2010). Szalai and Papp (2010) and Szalai (2017) recently clarified the theoretical background, and Hajdú and Papp (2018 and 2022) followed by systematic numerical validations making the General Method one of the most promising design methodologies of modern structural design standards.

3. Recommended Approach

The recommended approach providing the desirable qualities discussed in the previous sections is described below. An essential feature of the implementation is the use of strength-to-demand ratios – i.e., load multiplication factors – for the cross-section and buckling strengths. These ratios are necessary for handling general nonprismatic geometry and nonuniform loads.

Step 1   ***Perform an in-plane geometric nonlinear structural analysis using the DM.*** A specific form of the DM is recommended in Section 4.6.2 of DG25 and demonstrated and contrasted with other methods in its Ch. 7 through 10 frame design examples. White et al. (2022) summarize the rationale for the recommended procedure. The recommended method analyzes the structure with elastic stiffness reductions, typically $0.8E$. In addition, an out-of-plumbness is included in the analysis of the framing system for gravity-only load combinations in all cases, and for lateral-load combinations whenever the frame violates overall lateral sidesway stiffness criteria. Furthermore, an out-of-straightness is modeled in members whose axial forces exceed a certain threshold. In many typical metal building frames, no modeling of member out-of-straightness is necessary. The reader is referred to DG25 for the detailed requirements. When conducted according to these requirements, the structural analysis provides a sufficient estimate of the structure's internal forces such that the in-plane stability may be assessed on a cross-section by cross-section basis. These same forces are also appropriate for checking out-of-plane strengths, which often govern the member resistances. The out-of-plane limit states are evaluated by applying the member equations configured as discussed below.

Step 2   ***Determine cross-section strength-to-demand ratios and identify critical cross-sections.***
Given the forces from Step 1, calculate the cross-section strength-to-demand ratios

$$\gamma_s = \left(\frac{P_u}{2\phi_c P_{ns}} + \frac{M_u}{\phi_b M_{ns}} \right)^{-1} \text{ for } \frac{P_u}{\phi_c P_{ns}} \le 0.2 \;;\;\; \gamma_s = \left(\frac{P_u}{\phi_c P_{ns}} + \frac{8}{9}\frac{M_u}{\phi_b M_{ns}} \right)^{-1} \text{ otherwise} \tag{1}$$

throughout the structural system, and

$$\gamma_{sg} = \left(\frac{P_u}{P_y} + \frac{M_u}{M_{yc}} \right)^{-1} \tag{2}$$

at the member locations having the smallest γ_s, where P_u and M_u are the axial force and moment demands determined in Step 1, P_{ns} and M_{ns} are the cross-section axial and flexural capacities (for L_c and $L_b = 0$) considering any plate local buckling effects (and tension rupture effects for members subjected to tension), P_y and M_{yc} are the axial yield load and the yield moment to the compression flange for the gross cross-section, and ϕ_c and ϕ_b are the resistance factors for axial compression and flexure, equal to 0.9 (only LRFD is considered in this paper for simplicity). It is recommended that it is sufficient in all cases to identify the critical cross-section of a given member as the one with the smallest γ_s. Note, a form of Eq. 1 can be written for members subjected to axial tension.

Step 3   ***Determine the out-of-plane elastic buckling load-to-demand ratios.*** Given the in-plane forces from Step 1, determine the out-of-plane elastic buckling load-to-demand ratios for the different members, $\gamma_{e.op}$. Notably, the ratios $\gamma_{e.op}$ are simply the appropriate eigenvalues associated with the member out-of-plane buckling. Section 8 discusses the definition of what serves as a frame member and the calculation of different member $\gamma_{e.op}$ values using a buckling sensitivity analysis. Rough estimates of these eigenvalues can be determined from closed-form equations as illustrated in DG25. However, for complex member geometries, continuity considerations, end conditions, and out-of-plane bracing arrangements, $\gamma_{e.op}$ can be obtained most accurately and reliably by computation using 14-dof frame elements based on thin-walled open-section beam theory. Notably, $\gamma_{e.op}$ is a constant for any given member.

Step 4   ***Calculate the out-of-plane member slenderness.*** For each member, given the above γ_{sg} ratios at the critical member cross-sections (having the smallest γ_s for each member) and the $\gamma_{e.op}$ ratios (constants) for the members, calculate the out-of-plane slenderness as

$$\lambda_{op} = \sqrt{\frac{\gamma_{sg}}{\gamma_{e.op}}} \tag{3}$$

Step 5   ***Finalize the verification of the member strengths.*** For each member, calculate the axial and flexural resistances, P_n and M_n, using the slenderness defined in Eq. 3. Given the P_n and M_n values, the member verification is finalized by calculating the following "unity check" (*UC*) from Eqs. H1-1a and 1b of the AISC 360 *Specification*:

$$UC = \frac{P_u}{2\phi_c P_n} + \frac{M_u}{\phi_b M_n} \text{ for } \frac{P_u}{\phi_c P_n} \le 0.2 \;;\;\; UC = \frac{P_u}{\phi_c P_n} + \frac{8}{9}\frac{M_u}{\phi_b M_n} \text{ otherwise} \tag{4}$$

4. Adaptation of the AISC 360 Provisions

Slein et al. (2022 and 2023) and Latif and White (2021) have recommended several improvements to the AISC 360 flexural resistance calculations for built-up I-section members based on recent experimental and analytical investigations supplementing a large body of prior research. For doubly-symmetric I-section members, these improvements are as follows:

1) The inelastic/elastic (LTB) threshold is lowered from $R_{pg}M_L = 0.7R_{pg}M_{yc}$ to $0.5R_{pg}M_{yc}$, where R_{pg} is the web bend-buckling strength reduction factor for slender-web cross-sections in AISC 360 Note, $R_{pg} = 1.0$ for compact- and noncompact-web sections.
2) The compact-web limit (λ_{pw}) is determined using the more general equation for singly-symmetric I-sections in Case 16 of the AISC 360 Table B4-1b.
3) The noncompact-web limit (λ_{rw}) is calculated using the c_{rw} variable from AASHTO (2020) rather than a constant of 5.70. Correspondingly, the constant 5.70 also is replaced by c_{rw} in the AISC 360 equation for R_{pg}.
4) The flange local buckling (FLB) resistance in flexure is quantified by a simple linear equation having ordinates of $R_{pg}R_{pc}M_{yc}$ at $\lambda_f = b_{fc}/2t_{fc}$ equal to the AISC 360 compact-flange limit, λ_{pf}, and $0.75R_{pg}M_{yc}$ at λ_f equal to the AISC 360 noncompact-flange limit, λ_{rf}.

Notably, related provisions have been balloted and approved for the AASHTO (2023) 10th Edition *Specifications* that implement the above-recommended changes 1 through 3.

In addition, for singly-symmetric I-sections with a larger flange in compression (and thus $S_{xt} < S_{xc}$), Slein et al. (2022) recommend that the AISC 360 tension-flange yielding (TFY) provisions be eliminated and replaced by: (1) The calculation of M_{yc} as the "true" yield moment to the compression flange, considering the early yielding on the tension side of the cross-section, and (2) replacing the web parameter h_c by h_{cy}, defined as two times the depth of the web in compression corresponding to the actual yield moment. Straightforward closed-form equations are provided for M_{yc} and h_{cy}. Notably, M_{yc} is still defined as $F_{yc}S_{xc}$ and $h_{cy} = h_c$ for doubly-symmetric cross-sections and singly-symmetric cross-sections with $S_{xt} > S_{xc}$. These changes significantly simplify the flexural resistance calculations for singly-symmetric I-section members while accounting for the substantial inelastic reserve strength of I-sections with $S_{xt} < S_{xc}$. The reader is referred to Slein et al. (2022) for model *Specification* provisions and commentary implementing the recommendations.

All the above changes are being considered by AISC TC 4 for the 2027 *Specification* cycle. This paper implements these calculations. Furthermore, the above changes are applied to the DG25 provisions in the current study. The DG25 provisions supplement the AISC 360 *Specification*, addressing frame design using nonprismatic members and various characteristics of these frame types. Rather than writing the member axial compressive and flexural strengths in terms of corresponding effective unbraced lengths, DG25 uses the ratio of the yield stress to the theoretical elastic buckling strengths, $F_y/F_{e.op} = \lambda_{op}^2$, to calculate the member resistances P_n and M_n.

5. Prismatic Beam-Column Example

It is informative to consider the recommended calculations in the context of a simple prismatic beam-column example. As such, the member from DG25 Examples 5.2a, b, and c (see Fig. 2) is evaluated in this section by employing the top cross-section throughout its length (i.e., this section considers a prismatic version of the member shown in Fig. 2 in which the web is 24 in. deep throughout the member length). Section 6 shows the minor changes needed to address the strength

verification for the web-tapered member. All of the structural analysis solutions presented in this paper are conducted using the Consteel (2023) software.
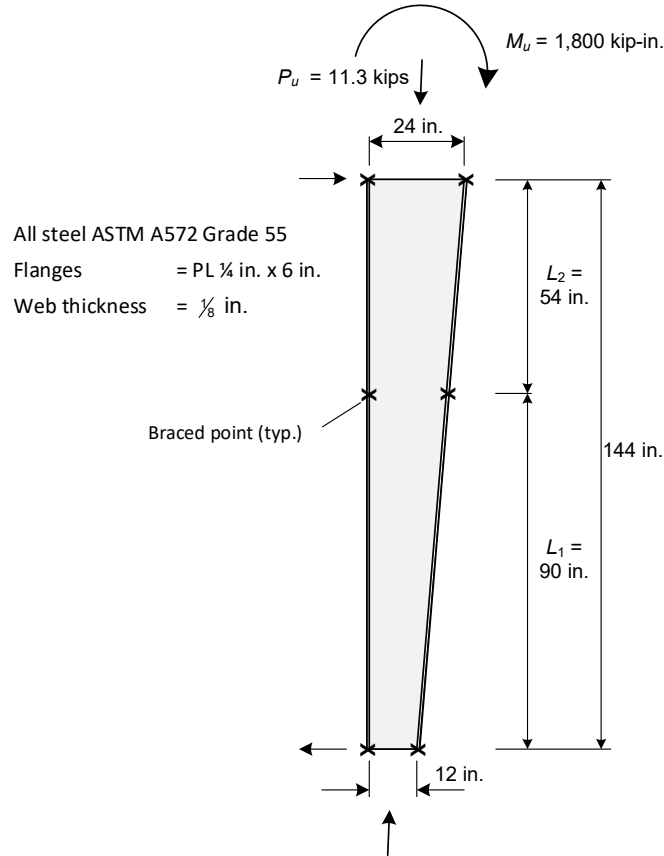

Figure 2: Web-tapered member from Examples 5.2a, 5.2b and 5.2c of the AISC/MBMA DG25 (White et al. 2021)

The strength check under axial compression alone is shown first, then the resistance under the applied bending moment alone is evaluated. These strength verifications are illustrated in the format described in Section 3; however, one can observe that these calculations match precisely with the AISC 360 provisions as amended in Section 4. Finally, the recommended strength verification under the combined axial compression and bending is discussed.

Strength Verification for Concentric Axial Compression Alone
(1) *Perform an in-plane geometric nonlinear structural analysis using the DM.* For this load case, it is assumed that the structural analysis has determined solely a concentric axial compression of $P_u = 11.3$ kips on the member (or the moment from the analysis is simply neglected).

(2) *Determine the cross-section strength-to-demand ratios and identify the critical cross-section.* All cross-sections are equally critical for a prismatic member subjected to constant axial compression. Applying the AISC Section E7 rules, the web effective width at $F_{cr} = F_y$ (corresponding to the cross-section strength) is $b_{ew} = 5.37$ in., and the flange effective widths are $b_{ef} = 4.94$ in., giving a cross-section effective area of $A_{es} = 3.14$ in.^{2}. Therefore,

$$P_{ns} = F_y A_{es} = 173 \text{ kips and } \gamma_s = \phi_c P_{ns}/P_u = 13.8 \tag{5}$$

Correspondingly, the gross cross-section strength-to-demand ratio is calculated as

$$P_y = F_y A_g = 330 \text{ kips and } \gamma_{sg} = P_y/P_u = 29.2 \tag{6}$$

(3) *Determine the out-of-plane elastic buckling load-to-demand ratio.* Using an eigenvalue buckling analysis, the out-of-plane elastic buckling load-to-demand ratio for the subject problem is obtained as

$$\gamma_{e.op} = 39.7 \tag{7}$$

That is, theoretical elastic buckling occurs for the prismatic version of the member shown in Fig. 2, subjected solely to a factored LRFD load of $P_u = 11.3$ kips, at 39.7 times the factored load (or $P_e = 448$ kips). The member buckling mode is flexural with the top unbraced length providing restraint to the bottom unbraced length. The corresponding effective length factor for the bottom segment can be calculated by equating P_e to $\pi^2 E I_y/(KL_1)^2$ and solving for K, giving $K = 0.842$. Similarly, $K = 1.41$ is obtained factor for the top segment.

(4) *Calculate the out-of-plane member slenderness.* The out-of-plane member slenderness for the subject problem is

$$\lambda_{op} = \sqrt{\frac{\gamma_{sg}}{\gamma_{e.op}}} = \sqrt{\frac{P_y}{P_e}} = \sqrt{\frac{F_y}{F_e}} = 0.858 \tag{8}$$

(5) *Finalize the verification of the member strength.* Given $\lambda_{op}^2 < 2.25$ in Eq. 8, the AISC 360 column strength in terms of stress is

$$F_{cr} = \left(0.658^{\lambda_{op}^2}\right) F_y = 40.4 \text{ ksi} \tag{9}$$

AISC 360 Section E7 estimates the axial compressive strength of members having slender cross-section elements using the unified effective width method. As such, the web and flange effective widths corresponding to F_{cr} are determined as $b_{ew} = 6.22$ in. and $b_{ef} = 5.46$ in., giving a cross-section effective area of $A_e = 3.51$ in^2. The axial compressive resistance is then calculated as

$$P_n = F_{cr} A_e = 142 \text{ kips} \tag{10}$$

Finally, the unity check is determined as

$$UC = \frac{P_u}{\phi_c P_n} = 0.089 \tag{11}$$

Strength Verification for Flexure Alone

(1) *Perform an in-plane geometric nonlinear structural analysis using the DM.* For this load case, it is assumed that the structural analysis has determined solely a moment of $M_u = 1800$ kip-in. at the top of the member (i.e., the axial compression is neglected).

(2) *Determine the cross-section strength-to-demand ratios and identify the critical cross-section.* Clearly, the cross-section moment demand on the prismatic member is largest at the top. Also, it can be observed that this is a slender-web member and that the compression flange in flexure is noncompact. The web slenderness is $h_{cy}/t_w = h/t_w = 192$,

$$a_w = \frac{h_{cy} t_w}{b_{fc} t_{fc}} = 2.00 \text{ and } c_{rw} = \min\left[\max\left(3.1 + \frac{5}{a_w}, 4.6\right), 5.7\right] = 5.6 \tag{12}$$

$$R_{pg} = 1 - \frac{a_w}{1200 + 300 a_w}\left(\frac{h_{cy}}{t_w} - c_{rw}\sqrt{\frac{E}{F_y}}\right) = 0.930 \tag{13}$$

and $R_{pc} = 1.00$. In addition, the cross-section FLB parameters are $k_c = 0.35$,

$$\lambda_f = \frac{b_{fc}}{2t_{fc}} = 12.0, \quad \lambda_{pf} = 0.38\sqrt{\frac{E}{F_y}} = 8.73 \text{ and } \lambda_{rf} = 1.14\sqrt{\frac{k_c E}{F_y}} = 15.5 \qquad (14)$$

Given the above parameters, the cross-section flexural strength, governed by FLB, is determined as

$$M_{ns} = R_{pg}\left[R_{pc}M_{yc} - \left(R_{pc}M_{yc} - 0.75M_{yc}\right)\left(\frac{\lambda_f - \lambda_{pf}}{\lambda_{rf} - \lambda_{pf}}\right)\right] = 2150 \text{ kip-in.} \qquad (15)$$

where $M_{yc} = 2630$ kip-in. Therefore, the critical cross-section strength-to-demand ratios are

$$\gamma_s = \frac{\phi_b M_{ns}}{M_u} = 1.07 \text{ and } \gamma_{sg} = \frac{M_{yc}}{M_u} = 1.46 \qquad (16)$$

(3) *Determine the out-of-plane elastic buckling load-to-demand ratio.* Using an eigenvalue buckling analysis and a 14-dof frame finite element based on thin-walled open-section beam theory, the elastic LTB load-to-demand ratio is obtained as

$$\gamma_{e.op} = 7.00 \qquad (17)$$

corresponding to an elastic LTB moment of $M_{cre} = 12{,}600$ kip-in. at the member's top. Upon substituting the appropriate values from the linearly-varying moment diagram in Eq. C-F1-2a of the AISC 360 commentary, one obtains a $C_b = 1.21$ for the top unbraced length of this member. If one substitutes this C_b and the relevant section properties into the theoretical elastic LTB moment equation and solves for the LTB effective length factor, $K_{LTB} = 1.02$ is obtained for this problem. This K_{LTB} indicates that the bottom unbraced length is slightly destabilizing the top unbraced length considering the flexural loading alone on the prismatic member.

(4) *Calculate the out-of-plane member slenderness.* The out-of-plane member slenderness for the subject problem is

$$\lambda_{op} = \sqrt{\frac{\gamma_{sg}}{\gamma_{e.op}}} = \sqrt{\frac{M_{yc}}{M_{cre}}} = \sqrt{\frac{F_y}{F_{eLTB}}} = 0.457 \qquad (18)$$

(5) *Finalize the verification of the member strength.* Using the modified AISC 360 LTB calculations recommended by Slein et al. (2022),

$$M_L = 0.5M_{yc} = 1310 \text{ kip-in.} \qquad (19)$$

and $8.16 > 1/\lambda_{op}^2 > 0.5$ such that the DG25 inelastic LTB resistance equation applies. Thus,

$$M_{nLTB} = R_{pg}R_{pc}M_{yc}\left[1 - \left(1 - \frac{M_L}{R_{pc}M_{yc}}\right)\left(\frac{\pi\lambda_{op} - 1.1}{\pi\sqrt{\frac{M_{yc}}{M_L}} - 1.1}\right)\right] = 2320 \text{ kip-in.} \qquad (20)$$

Given this value of M_{nLTB}, the flexural resistance of the member is governed by FLB, i.e.,

$$M_n = \min\left(M_{ns}, M_{nLTB}\right) = 2150 \text{ kip-in.} \qquad (21)$$

and

$$UC = \frac{M_u}{\phi_b M_n} = 0.932 \qquad (22)$$

Recommended Strength Verification under Combined Axial Compression and Flexure

(1) *Perform an in-plane geometric nonlinear structural analysis using the DM.* For this load case, it is assumed that the structural analysis has determined the axial load of $P_u = 11.3$ kips and $M_u = 1800$ kip-in. at the top of the prismatic version of the member shown in Fig. 2.

(2) *Determine the cross-section strength-to-demand ratios and identify the critical cross-section.* Clearly, the maximum cross-section demand (i.e., smallest γ_s) is again at the member's top. Utilizing the calculations shown previously, the critical cross-section strength-to-demand ratios are, since $P_u / \phi_c P_{ns} < 0.2$,

$$\gamma_s = \left(\frac{P_u}{2\phi_c P_{ns}} + \frac{M_u}{\phi_b M_{ns}} \right)^{-1} = 1.04 \text{ and } \gamma_{sg} = \left(\frac{P_u}{P_y} + \frac{M_u}{M_{yc}} \right)^{-1} = 1.39 \tag{23}$$

(3) *Determine the out-of-plane elastic buckling load-to-demand ratio.* Using an eigenvalue buckling analysis and a 14-dof frame finite element based on thin-walled open-section beam theory, the elastic out-of-plane buckling load-to-demand ratio is

$$\gamma_{e.op} = 6.26 \tag{24}$$

Note that this ratio is smaller than each of the above ratios for axial compression and flexure alone.

(4) *Calculate the out-of-plane member slenderness.* The out-of-plane member slenderness for the prismatic member subjected to combined axial compression and bending is

$$\lambda_{op} = \sqrt{\frac{\gamma_{sg}}{\gamma_{e.op}}} = 0.471 \tag{25}$$

(5) *Finalize the verification of the member strength.* Given the above value of λ_{op} determined for the combined loading, the axial compressive strength in terms of stress is calculated as

$$F_{cr} = \left(0.658^{\lambda_{op}^2} \right) F_y = 50.1 \text{ ksi} \tag{26}$$

The web and flange effective widths corresponding to F_{cr} are then determined as $b_{ew} = 5.61$ in. and $b_{ef} = 5.10$ in., giving a cross-section effective area of $A_e = 3.25$ in^2. Therefore, the axial compressive resistance is calculated as

$$P_n = F_{cr} A_e = 163 \text{ kips} \tag{27}$$

Similarly, the LTB resistance in flexure is calculated as

$$M_{nLTB} = R_{pg} R_{pc} M_{yc} \left[1 - \left(1 - \frac{M_L}{R_{pc} M_{yc}} \right) \left(\frac{\pi \lambda_{op} - 1.1}{\pi \sqrt{\frac{M_{yc}}{M_L}} - 1.1} \right) \right] = 2300 \text{ kip-in.} \tag{28}$$

Again, the flexural resistance for this member is governed by FLB:

$$M_n = \min \left(M_{ns}, M_{nLTB} \right) = 2150 \text{ kip-in.} \tag{29}$$

Finally, the unity check for the prismatic version of the member shown in Fig. 2 is

$$UC = \frac{P_u}{2\phi_c P_n} + \frac{M_u}{\phi_b M_n} = 0.970 \tag{30}$$

10

6. Web-Tapered Beam-Column Example

The calculations for the web-tapered beam-column shown in Fig. 2 are practically the same as those illustrated above for the prismatic version of this member. For the web-tapered member subjected to the combined axial compression and flexure, the critical cross-section is still at the top and the only difference in the calculations is that, in Step 3,

$$\gamma_{e.op} = 5.05 \tag{31}$$

due to the reduced out-of-plane buckling resistance associated with the linearly-tapered geometry. This results in

$$\lambda_{op} = \sqrt{\frac{\gamma_{sg}}{\gamma_{e.op}}} = 0.525 \tag{32}$$

in Step 4, and

$$F_{cr} = \left(0.658^{\lambda_{op}^2}\right)F_y = 49.0 \text{ ksi} \text{ and } b_{ew} = 5.67 \text{ in., } b_{ef} = 5.14 \text{ in., } A_e = 3.28 \text{ in.}^2, \tag{33}$$

$$P_n = F_{cr}A_e = 161 \text{ kips} \tag{34}$$

$$M_{nLTB} = R_{pg}R_{pc}M_{yc}\left[1 - \left(1 - \frac{M_L}{R_{pc}M_{yc}}\right)\left(\frac{\pi\lambda_{op} - 1.1}{\pi\sqrt{\frac{M_{yc}}{M_L}} - 1.1}\right)\right] = 2240 \text{ kip-in.} \tag{35}$$

$$M_n = \min\left(M_{ns}, M_{nLTB}\right) = 2150 \text{ kip-in.} \tag{36}$$

and

$$UC = \frac{P_u}{2\phi_c P_n} + \frac{M_u}{\phi_b M_n} = 0.971 \tag{37}$$

in Step 5.

7. Complex Metal Building Frame Example

This section highlights the member strength verifications by the recommended procedures for the DG25 clear-span crane-building frame shown in Fig. 1. The specifics of the cross-section geometries for this frame are listed in Table 1. DG25 describes the structure in detail.

The crane-building frame's unfactored design loads are shown in Fig. 1. DG25 evaluates this structure for the ASD load combination Dead + Collateral + 0.75 Uniform snow + the specified Crane loading. In the current study, a pseudo-LRFD ultimate strength load combination is considered by multiplying the applied loads from the ASD load combination by 1.6.

The member strength verifications for both the critical crane column and roof girder on the right-hand side of the frame (given the specified loads) are discussed in the following:

(1) *Perform an in-plane geometric nonlinear structural analysis using the DM.* For the in-plane second-order geometric nonlinear analysis of this frame, the DM requires a reduced elastic stiffness of $0.8E = 23,200$ ksi for all of the structural components included in the analysis model. However, no modeling of geometric imperfections is required. This is because:
 a. The load combination considered includes lateral load due to the horizontal crane loads; furthermore, the second-order amplification of the sidesway for the frame, modeled using

11

the reduced elastic stiffness, is less than 1.7. The reader is referred to Section 6.3.3 of DG25 for guidance on assessing the sidesway amplification for gabled clear-span portal frames.

b. The value of the in-plane elastic buckling load-to-demand ratios, γ_{eL}, is greater than 10 for all the members in this frame, considering them as simply supported at their ends and subjected solely to the axial compression. For this calculation, the column lengths are measured from the base of the frame to the bottom of the panel zones at the knees, and the roof girder length is taken as the length between the insides of the panel zones. Therefore, no in-plane out-of-straightness needs to be considered for the members. The reader is referred to Section 4.6.2 of DG25 for guidance in properly assessing whether member out-of-straightness needs to be modeled within the in-plane geometric nonlinear analysis.

The members and the panel zones at the knees of the frame are modeled as discussed in Section 8. Figures 3 and 4 show the frame moment and axial force diagrams, respectively, with the demands labeled at the critical member cross-sections. These diagrams are obtained from a geometric nonlinear analysis under a pseudo-LRFD ultimate strength loading performed according to the DM requirements (i.e., basically just a reduction of 0.8 applied to all the elastic stiffnesses in this example; an out-of-plumbness imperfection was also included, but its effects are small compared to the influence of the two 1.74-kip lateral loads factored by 1.6).

Table 1: Cross-section geometry of the clear-span crane-building frame

Segment	Length (ft)	Inside or Bottom Flg. b_f x t_f (in.)	Outside or Top Flg. b_f x t_f (in.)	Starting Web Depth h (in.)	Ending Web Depth h (in.)	t_w (in.)
A	11.948	8 x 1.00	8 x 0.75	16	27	0.1875
B	9.354	8 x 1.00	8 x 0.75	27	27	0.25
C1[1]	0.354	8 x 1.00	8 x 0.75	27	27	0.3125
C2[2]	2.709	8 x 1.00	8 x 0.75	27	27	0.3125
C3[3, 4]	2.189	7.3125 x 0.3125	8 x 0.75	31.811	34	0.3125
D	8.265	8 x 0.625	8 x 0.3125	34	36.312	0.25
E	5.958	8 x 0.50	8 x 0.3125	36.312	38	0.1875
F	11.917	8 x 0.3125	8 x 0.3125	38	24	0.1875
G	11.075	8 x 0.3125	8 x 0.3125	24	24	0.1345[5]
H1[6]	2.333	7.25 x 0.50	9.25 x 0.50	15.5	15.5	0.25
H2[7]	1.271	8 x 0.375	8 x 0.375	15.25	15.25	0.25

[1] Segment C1 is a short length located just below the column panel zone.

[2] Segment C2 describes a column segment oriented along the height of the column panel zone. The effective flanges of this cross section are composed of the outside column flange on the left and an end-plate connection composed of two 1.00 in. thick end plates on the right. Only one of these end plates is considered in the structural analysis of the frame.

[3] Segment C3 describes a roof girder segment oriented along the width of the column panel zone. The effective flanges of this cross section are composed of an end plate along the roof slope at the top of the panel and two-sided stiffeners oriented horizontally at the bottom of the panel. The effective bottom flange width of this segment is taken as the sum of the stiffener widths plus the thickness of the web.

[4] The start of segment C3 is taken as the intersection of the left edge of the column web and the roof girder design axis. The end of segment C3 is taken as the right-hand face of the two 1.00 in. plates of the end plate connection to the roof girder. There is a small offset of the top of the web in the column panel zone, which accommodates the thickness change between the top flange of the roof girder and the end plate at the top of the column panel zone (such that the top surface of the end plate at the top of the column and the top surface of the roof girder fall along a straight line). This offset is neglected for modeling purposes, such that the top edge of the column web and the top edge of the roof girder web fall along a straight line in the analysis model.

[5] The dimension 0.1345 in. corresponds to 10 gauge steel sheet.

[6] Segment H1 is an effective section composed of the column web and the two-sided stiffener (continuity) plates between the column flanges, located approximately at the level of the flanges of the crane girder support bracket.

[7] Segment H2 is the crane girder support bracket.

(2) *Determine the cross-section strength-to-demand ratios and identify the critical cross-sections.* For the strength verifications, the lengths from the column bases to the bottom of the panel zones are considered as the column members, and the lengths from the inside of the panel zones to the ridge are considered as the roof girders. For the specified ultimate strength load combination, the critical member cross-sections (i.e., the ones having the smallest values of γ_s), are located on the right-hand side of the frame at the bottom of the panel zone for the crane columns and at the inside of the panel zone for the roof girders. The detailed member strength verifications for the crane columns are shown below.

M_u = 4311 kip-in., critical cross-section at inside of panel zone at knee

M_u = 4337 kip-in., critical cross-section at bottom of panel zone at knee
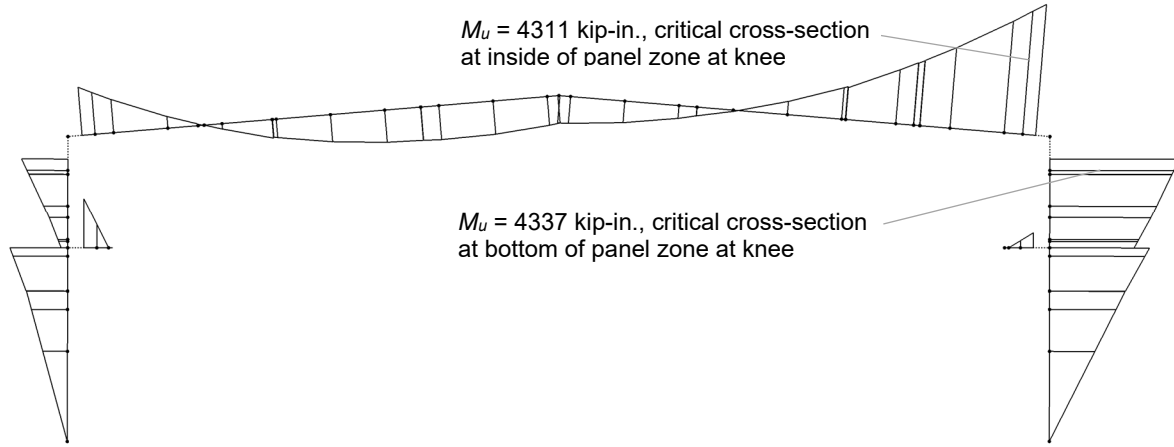
Figure 3: Clear-span crane-building frame moment diagram under specified factored loads

P_u = 20.5 kips, critical cross-section at inside of panel zone at knee

P_u = 26.0 kips, critical cross-section at bottom of panel zone at knee
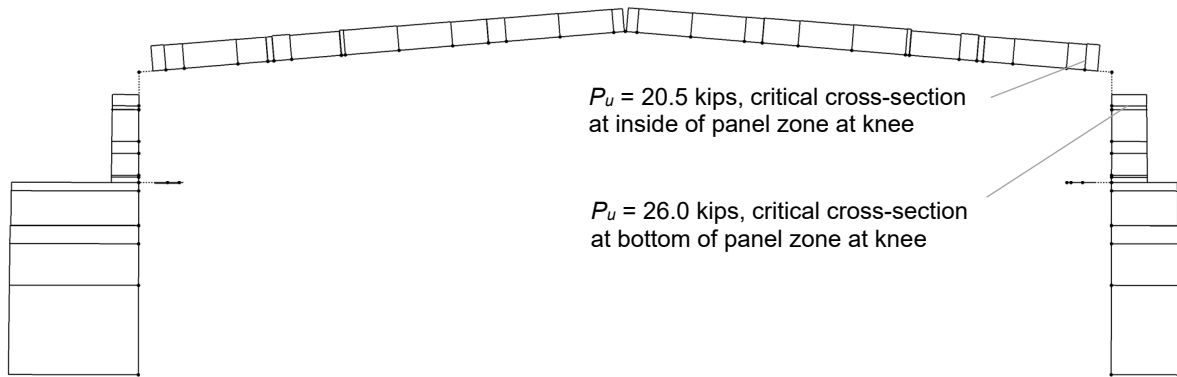
Figure 4: Clear-span crane-building frame axial force diagram under specified factored loads

For the critical cross-section at the top of the crane column, h/t_w = 108 and the web effective width at $F_{cr} = F_y$ (corresponding to the cross-section strength) is b_{ew} = 10.4 in. However, both flanges of this cross-section are nonslender under axial compression and therefore $b_{ef} = b_f$ = 8.0 in. for both flanges. The resulting A_{es} is 16.6 in.^{2} and

$$P_{ns} = F_y A_{es} = 913 \text{ kips and } P_y = F_y A_g = 1140 \text{ kips} \tag{38}$$

At this cross-section, the traditional calculation of the yield moment as $F_y S_{xc}$ is actually larger than the plastic moment. This anomaly is to the lack of consideration of the early yielding in flexural tension. The true yield moment to the compression flange, considering the early yielding in tension, may be calculated by first determining the corresponding location of the neutral axis from the outside surface of the compression flange as

$$d_{cy} = \frac{\Delta A + \sqrt{\Delta A^2 + 2 A_{fc} A_{wfc} - A_{wfc}^2}}{4 t_w} = 11.19 \text{ in.} \tag{39}$$

where

$$\Delta A = A_{ft} + A_w + A_{wfc} - A_{fc}, \ \ A_{wfc} = 2 t_{fc} t_w, \ \ A_{ft} = b_{ft} t_{ft}, \ \ A_w = h t_w, \ \text{ and } \ \ A_{fc} = b_{fc} t_{fc} \tag{40}$$

Then, given that $2d_{cy} < h + t_{fc}$, the true yield moment is calculated as

$$M_{yc} = F_y \left[\frac{A_{fc}}{d_{cy}} \left(\frac{D_{cy} t_{fc}}{2} + \frac{t_{fc}^3}{3} \right) + A_{ft} \left(h + \frac{t_{ft}}{2} \right) + \frac{t_w}{2} \left(h^2 - t_{fc}^2 - \frac{7 d_{cy}^2}{3} + 3 d_{cy} t_{fc} - \frac{D_{cy}^3}{3 d_{cy}} \right) \right]$$
$$= 12,300 \text{ kip-in} \tag{41}$$

where

$$D_{cy} = d_{cy} - t_{fc} = 10.19 \text{ in.} \tag{42}$$

is the depth of the web in compression corresponding to the true yield moment. The comparable depth of the web in compression at the plastic moment level is

$$D_p = \frac{A_w + A_{ft} - A_{fc}}{2 t_w} = 9.5 \text{ in.} \tag{43}$$

and the cross-section plastic moment is calculated as

$$M_p = F_y \left[A_{fc} \left(D_p + \frac{t_{fc}}{2} \right) + \frac{t_w D_p^2}{2} + \frac{t_w (h - D_p)^2}{2} + A_{ft} \left(h - D_p + \frac{t_{ft}}{2} \right) \right] = 13,000 \text{ kip-in} \tag{44}$$

Given the above parameters, the noncompact-web limit is determined as

$$h_{cy} = 2 D_{cy}, \ \ a_w = \frac{h_{cy} t_w}{b_{fc} t_{fc}}, \ \ c_{rw} = \min \left[\max \left(3.1 + \frac{5}{a_w}, 4.6 \right), 5.7 \right] = 5.7, \ \ \lambda_{rw} = c_{rw} \sqrt{\frac{E}{F_y}} = 131 \tag{45}$$

and the compact-web limit is calculated as

$$h_p = 2 D_p, \ \ \lambda_{pw} = \min \left[\frac{\frac{h_{cy}}{h_p} \sqrt{\frac{E}{F_y}}}{\left(0.54 \frac{M_p}{M_{yc}} - 0.09 \right)^2}, \ \lambda_{rw} \right] = 105 \tag{46}$$

Finally, the web slenderness, defined as $h_{cy}/t_w = 81.5$, is smaller than λ_{pw}, and therefore the web is classified as compact. Given that the compression flange is also compact, the cross-section flexural resistance, M_{ns}, is equal to the plastic moment, M_p. As such, the cross-section strength-to-demand ratios are calculated as, considering $P_u/\phi_c P_{ns} < 0.2$,

$$\gamma_s = \left(\frac{P_u}{2 \phi_c P_{ns}} + \frac{M_u}{\phi_b M_{ns}} \right)^{-1} = 2.59 \text{ and } \gamma_{sg} = \left(\frac{P_u}{P_y} + \frac{M_u}{M_{yc}} \right)^{-1} = 2.66 \tag{47}$$

The reader is referred to Slein et al. (2022) for model *Specification* provisions and commentary implementing the calculations.

(3) *Determine the out-of-plane elastic buckling load-to-demand ratio.* Using an eigenvalue buckling analysis and a 14-dof frame finite element based on thin-walled open-section beam theory, the elastic out-of-plane buckling load-to-demand ratio for the combined axial compression and flexural loadings is

$$\gamma_{e.op} = 9.24 \tag{48}$$

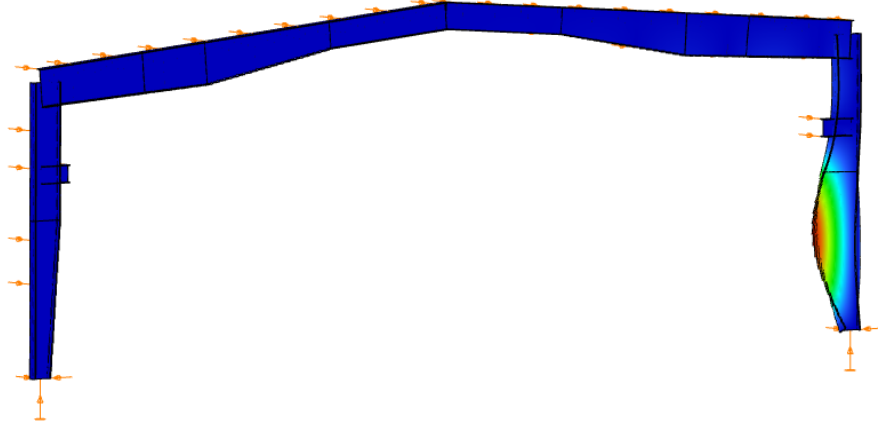for the crane column. Figure 5 shows the corresponding buckling mode. The contours indicate the magnitude of the out-of-plane displacements in this mode.

Figure 5: Out-of-plane buckling mode for the right-hand column in the clear-span crane-building frame

(4) *Calculate the out-of-plane member slenderness.* The out-of-plane member slenderness for crane column, subjected to combined axial compression and bending, is

$$\lambda_{op} = \sqrt{\frac{\gamma_{sg}}{\gamma_{e.op}}} = 0.536 \tag{49}$$

(5) *Finalize the verification of the member strength.* Given the above value of λ_{op} determined for the combined loading, the crane column axial compressive strength in terms of stress is

$$F_{cr} = \left(0.658^{\lambda_{op}^2}\right)F_y = 48.8 \text{ ksi} \tag{50}$$

The web effective width corresponding to F_{cr} is then determined as $b_{ew} = 11.0$ in. while the flanges are nonslender and fully effective under axial compression. This results in a cross-section effective area of $A_e = 16.7 \text{ in}^2$ and an axial compressive resistance of

$$P_n = F_{cr}\,A_e = 816 \text{ kips} \tag{51}$$

Similarly, the resistance in flexure, which is governed by LTB, is;

$$M_n = R_{pg}R_{pc}M_{yc}\left[1-\left(1-\frac{M_L}{R_{pc}M_{yc}}\right)\left(\frac{\pi\lambda_{op}-1.1}{\pi\sqrt{\frac{M_{yc}}{M_L}}-1.1}\right)\right] = 11{,}800 \text{ kip-in.} \tag{52}$$

where $R_{pg} = 1.00$, $R_{pc} = M_p/M_{yc} = 1.06$ since the web is compact, and $M_L = 0.5M_{yc} = 6130$ kip-in. Finally, the unity check for the crane column is determined as

$$UC = \frac{P_u}{2\phi_c P_n} + \frac{M_u}{\phi_b M_n} = 0.425 \tag{53}$$

It is notable that the current provisions in AISC 360 and DG25 for the above member are limited by the highly-conservative TFY limit state calculation. The above calculations recognize the substantial inelastic reserve capacity that singly-symmetric I-section members with a larger flange subjected to flexural compression can have.

The calculations for Steps 2 through 5 of the roof girder are similar to the above crane-column calculations. However, the roof girder web classifies as noncompact for the critical cross-section located at the inside of the knee. The Step 3 governing elastic out-of-plane buckling mode for the roof girder is shown in Fig. 6. The buckling load-to-demand ratio is $\gamma_{e.op} = 12.94$ and the final unity check value for the roof girder is $UC = 0.485$.
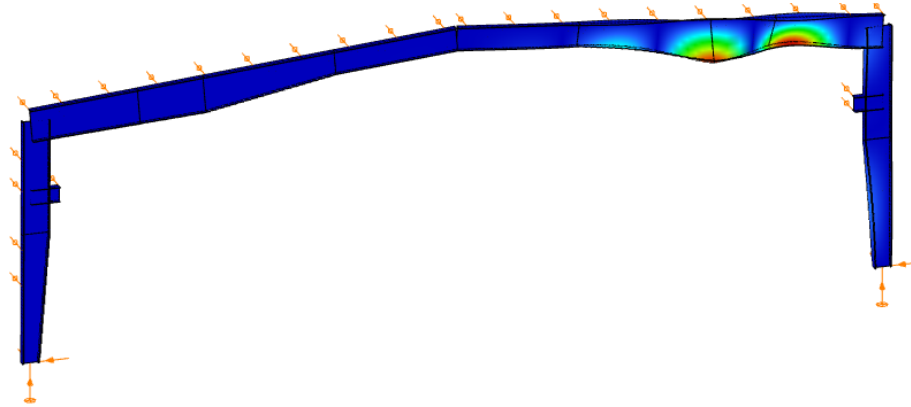
Figure 6: Out-of-plane buckling mode for the right-hand portion of the roof girder, clear-span crane-building frame

8. Software Considerations

For the most effective implementation of the recommended design approach, computer software is required. To perform the necessary calculations, 14-dof beam-column finite elements based on thin-walled open-section beam theory are needed. One essential attribute of these element types is the proper consistent linearization of the nonlinear equations as well as the handling of nonprismatic member geometry (i.e., variations in the cross-section geometry along the length). DG25 Appendix C1 discusses the essential software features necessary for these frame elements.

Another essential attribute is the modelling of the compatibility between members with different cross-sections where special attention is needed to address the warping continuity between the members. For typical metal building frames, the knee joint between the exterior columns and the roof girders is one of the most important locations exposed to this problem. This is because the knee joint typically has the deepest sections and the largest internal moments. At this location, the transfer of warping deformations between the columns and roof girders also involves cross-section distortion.

It can be shown that the topology of the connection at the knee joints significantly influences the rate and direction of the transfer of warping deformations across this zone. Figure 7 shows the differences in the deformations associated with out-of-plane displacements at several representative knee joints. Several possibilities are recommended in the literature addressing the definition of knee joints and the transfer of warping deformations with 14-DOF beam finite elements using multi-point constraint (MPC) equations parametrized as a function of the most common joint topologies (Basaglia et al. 2012).
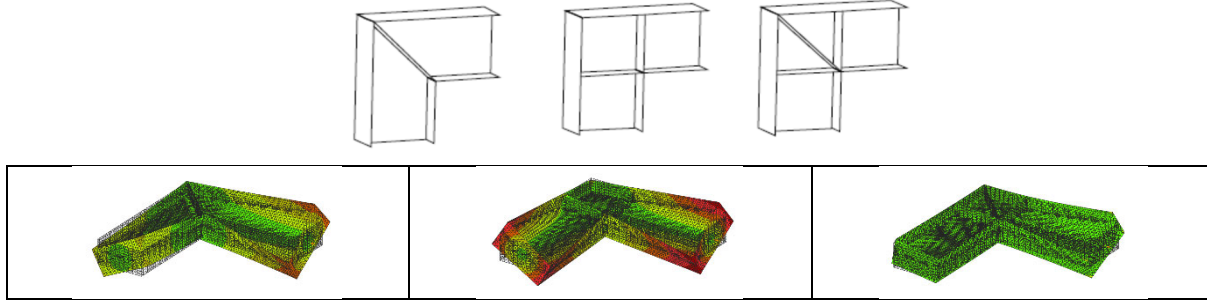
16

Figure 7: Representative knee joint topologies showing the corresponding deformations under the application of torsion

In addition, for less common connection configurations, a general approach may be employed for modelling the joint region using suitable beam and/or shell finite elements (Vaszilievits-Sömjén and Szalai 2018; Vaszilievits-Sömjén and Szalai 2019) or shell elements (MacPhedran and Grondin 2009; Wu and Mohareb 2013; Koczubiej and Cichon 2014; Shayan and Rasmussen 2014), linked via MPC equations at the boundaries of the joint to members modelled with 14-dof beam-column finite elements . Figure 8 illustrates this concept. Consteel (2023) is one example of professional software that provides all of the above capabilities.
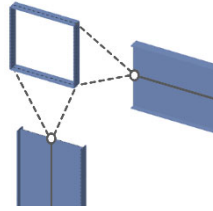

Figure 8: System composed of a panel zone molded by suitable beam and/or shell finite elements and connected members modeled using 14-dof frame finite elements

Another consideration in the application of eigenvalue buckling methods for assessing out-of-plane stability is the question of "what is a member?" In the examples shown in Sections 5 and 6, it is common that the member would be defined as the entire length between the beam-column bottom and top. However, in general, any particular length may be considered as a member. Given the member definitions, the elastic buckling modes of a system are calculated using the global structural model, considering the continuity between its members. The most effective application of the General Method requires the consideration of the most relevant buckling mode and the corresponding critical elastic load factor for the proper stability design of the member under examination. In the case of a complex 3D structural model with a large number of different but relevant buckling modes it is usually not evident which is the most relevant mode for the design of a certain member (Szalai 2010). This is a relevancy problem. It is common, that different buckling modes describe the stability behavior of distinct parts of the model. For that reason, a scaling procedure may be employed to facilitate the selection of the appropriate buckling mode for the stability design of different members. The deformation energy generated by the ith buckling mode is used as a basic measure, formulated as follows:

$$E_i = \tfrac{1}{2} \sum \mathbf{v}^T \mathbf{K}_s \mathbf{v} \qquad (54)$$

where $\mathbf{v}$ is the vector of nodal displacements of the actual buckling mode shape, $\mathbf{K}_s$ is the member stiffness matrix compiled from the elementary 14x14 element stiffness matrices, and E_i is the deformation energy of the ith member within the structural system.

Using these measures, a specific scaling procedure can be constructed defining a so-called mode relevance factor (MRF), which identifies which members are considered relevant (critical) for the ith buckling mode. The basic assumption for this factor is that each buckling mode has one or more specific members which are the most critical, and all the members are compared to these members to assess the contribution to the buckling:

$$MRF_i = \frac{E_i}{\max(E_i)} 100 \tag{55}$$

For the most critical member this factor always takes exactly 100%, and the more critical a member the closer is the *MRF* to 100%. The buckling mode shape is considered as irrelevant for members where the *MRF* factor falls below minimum threshold. Consteel (2023) provides one implementation of these capabilities.

9. Comparison of AISC 360-DG25 and Eurocode 3 Details

During the preparation of this paper, several philosophical and technical differences between AISC 360 and Eurocode 3 have been observed. The following summary is offered in the spirit of further development of both standards and possible harmonization between them.

Eurocode 3 defines the buckling resistance of compressed members and members subject to bending in a similar way. This is not the case in AISC 360, where member strengths in the case of compression and flexure are defined differently. Eurocode 3 defines one single limit state for both cases. AISC 360 defines similarly one single limit state for compression but defines multiple limit states for flexure. That is, FLB is addressed as part of the overall axial compressive resistance but is defined as an independent limit state for flexure. There is experimental evidence for handling FLB as a limit state independent of LTB for practical I-section geometries (Latif and White 2021). Whether this evidence is sufficient to justify a different form of the resistance calculations for flexure could be given further scrutiny.

Eurocode 3 uses multiple strength curves both for compression and bending following the Ayrton-Perry concepts. The reduction factors χ and χ_{LT} are defined based on a nondimensional slenderness parameter similar to λ_{op}. However, the nondimensional slenderness term is always taken as a ratio relative to the maximum cross-section strength in Eurocode 3. Conversely, the comparable term in AISC 360/DG25 is the yield axial load or yield moment on the gross cross-section.

In Eurocode 3, the member buckling resistance is calculated by multiplying the cross-section resistance by the above reduction factors. The Eurocode 3 use of cross-section resistance with a single reduction factor including the effect of all relevant limit states allows for an elegant formalization of the resistance equations. In contrast, the AISC 360 buckling resistance of slender-element members is not just a simple reduction applied the cross-section resistance. The unified effective width approach in AISC 360 is based on the concept that the axial compressive strength, in terms of stress, can be based sufficiently on the gross cross-section properties, and that the plate effective widths tend to be larger when the member fails at a smaller nominal axial stress level. The Eurocode 3 approach for calculation of the axial compressive strength is based more on the concept that the maximum plate stress is essentially at F_y due to axial compression and amplified bending, at the limit of the resistance. Therefore, one calculates the Eurocode 3 cross-section strength using plate effective widths based on F_y, identifies the proper selection from the multiple strength curves, and assumes there is no impact of member overall slenderness on the plate effective widths.

In the design approach illustrated in this paper, it is recommended that the critical cross-section for a given member verification should be taken as the cross-section having the smallest strength-to-demand ratio, γ_s (see Eq. 1). In the Eurocode 3 approach, the cross-section with the minimum γ_s always gives the largest unity check (since the cross-section strength is simply reduced by χ and χ_{LT} as a function of the member's slenderness in the Eurocode 3 equations). However, the largest unity check from the AISC 360/DG25 calculations potentially can occur at a cross-section other than the one with the minimum γ_s. Nevertheless, the difference in the unity check determined by performing the full member strength verifications at a number of different cross-sections (as recommended in DG25) versus the value obtained using just the cross-section having the minimum γ_s is small. Therefore, it is recommended that the unity check value obtained using solely the cross-section with the minimum γ_s is good enough. In the limit that the member slenderness approaches zero, one always obtains the cross-section strength in both Eurocode 3 and DG25.

In a traditional design according to Eurocode 3, there are typically two different slenderness values used in determining member buckling resistances, one for compression and one for bending. In the General Method, only one common slenderness value is used for both buckling resistance calculations. AISC 360 uses a similar term (F_y / F_e) for compression (similar at least in the case of members where all the cross-section elements are nonslender). For flexure, the AISC 360 approach is different and is based on the physical length of the beam between braced locations. DG25 has introduced an alternative formulation of the AISC 360 strength equations based on the slenderness concept.

In the case of cross-sections with slender components, Eurocode 3 classifies the whole cross-section as Class 4; however, AISC considers individual slender elements within the cross-section.

Eurocode 3 uses the effective width concept for the design of Class 4 sections both in compression and in flexure, traditionally by applying pure compression and pure bending cases separately, but alternatively also together. Alternatively, AISC uses the effective width approach explicitly only for compression, not for flexure. The R_{pg} term for calculation of the resistance of slender-web members in flexure was developed as a coarse representation of the cross-section bending resistance considering the loss of effectiveness and post-buckling action of the web. The use of this term allows for the calculation of flexural resistance for slender-web members in a single step. Conversely, the most rigorous Eurocode 3 calculation of the flexural resistance for a cross-section with a Class 4 web requires iteration.

According to Eurocode 3, the slenderness parameter for the buckling resistance of a Class 4 section is calculated based on the effective cross-section. In contrast, AISC uses the gross section properties for its slenderness-like parameter, justified based on the logic of the unified effective width approach.

The lateral-torsional buckling resistance calculated based on Eurocode 3 rules for welded sections is substantially smaller than the same value according to AISC, even in the case of uniform moment distribution. One reason for this behavior is the use of a conservative buckling curve proposed by Eurocode 3 for welded sections, accounting for the possibility of higher residual stresses. It is also due to the way inelastic LTB strengths are defined in AISC. In the case of nonuniform bending moment application, handled by the elastically-determined C_b factor and used directly in the AISC LTB equation, this difference becomes even more significant. Evidence from recent experimental and analytical research (Phillips et al. 2023a and b) indicates that it can be

significantly unconservative to scale the LTB resistance of thinner-web members by the elastically-derived C_b factor to strength levels where significant on-set of yielding would be expected. The DG25 approach discussed in this paper applies the C_b factor only for manual estimation of the elastic buckling moment or flexural stress.

The General Method implementation as presented in this paper is based on fundamental principles and therefore accepts the differences between these standards. Further validation of this approach versus experimental test results and test simulations would be appropriate. The predicted strengths are in line with results obtained by a traditional design based on either Eurocode 3 or AISC 360. Further comparison of the efficacy of the Eurocode 3 and AISC 360 approaches at large with respect to their ability to predict experimental and simulation-based resistances as well as their ease (speed) of use would be of interest

10. Conclusion

Researchers and practicing engineers have made significant progress in developing highly effective methods for designing nonprismatic members and frames composed of such members. For example, the Eurocode 3 Part 1-1 provides a so-called General Method that generalizes its rules for member proportioning, while the AISC/MBMA Design Guide 25 (DG25) provides extensions to the AISC 360 *Specification*. Furthermore, recent research has proposed advancements in the AISC 360/DG25 calculations providing improved accuracy, simplicity, and transparency. This paper shows how the best practices and procedures from the recent work in Europe and the US can be combined to provide rational and economical calculations addressing the complexities of frame designs using nonprismatic members with maximum design speed. The specific recommendations include: (1) Apply specific DG25 Direct Analysis Method (DM) rules that capture the in-plane stability effects in a manner such that the in-plane stability may be assessed on a cross-section by cross-section basis; (2) In the first step of the member design verifications, identify the single critical cross-section within each member for the design checks as the one having the minimum cross-section strength-to-demand ratio; (3) At least in the final design verification stages, determine the appropriate critical out-of-plane elastic buckling load-to-demand ratios for each member using 14-dof frame finite elements that handle the essential aspects associated with the variations in the cross-section geometries along the member lengths as well as the general positioning of brace points and the warping and other continuity effects at structural joints; (4) Utilize the General Method for the member verifications, considering the actual behavior under the combined loading effects explicitly and realistically; and (5) Implement the improvements to the AISC 360 procedures recommended in recent research, which eliminate the need to consider a tension flange yielding (TFY) limit state while providing a number of additional enhancements in the strength predictions.

References
AASHTO (2020). *AASHTO LRFD Bridge Design Specifications*, 9th Ed., American Association of State and Highway Transportation Officials, Washington, D.C.
AASHTO (2023). *AASHTO LRFD Bridge Design Specifications*, 10th Ed., American Association of State and Highway Transportation Officials, Washington, D.C., (to appear).

AISC (2022). *Specification for Structural Steel Buildings*, ANSI/AISC 360-22, American Institute of Steel Construction, Chicago, IL.

Basaglia C., Camotim, D., Silvestre, N. (2012). "Torsion, warping transmission at thin-walled frame joints: Kinematics, modelling and structural response," *Journal of Constructional Steel Research*, 69(1), 39-53, doi:10.1016/j.jcsr.2011.07.016.

Bijlaard, F., Feldmann, M., Naumes, J., & Sedlacek, G. (2010). "The 'general method' for assessing the out-of-plane stability of structural members and frames and the comparison with alternative rules in EN 1993 - Eurocode 3 - Part 1-1." Steel Construction, 3(1), 19–33. doi:10.1002/stco.20101000.

CEN (2005). *Eurocode 3: Design of Steel Structures – Part 1-1: General Rules and Rules for Buildings*, EN 1993-1-1:2005, Comité Européen de Normalisation.

Consteel (2023), www.consteelsoftware.com.

Hajdú G, Papp F. (2018), "Safety assessment of different stability design rules for beam-columns", Structures, 14, 376–388.

Hajdú, G. Papp, F. (2022). "On the accuracy of general method adapted in EN 1993-1-1." Journal of Constructional Steel Research. 195. 107354. 10.1016/j.jcsr.2022.107354.

Phillips, M., Slein, R., Sherman, R.J., White, D.W. (2023a). "Experimental investigation of doubly-symmetric built-up I-girders subjected to high moment gradient," *Engineering Structures*, in press.

Phillips, M., Kamath, A.M., Sherman, R.J., White, D.W. (2023b). "Influence of web distortion and onset of yield on doubly symmetric built-up I-girders subjected to high moment gradient," *Thin-Walled Structures*, 185, doi/10.1016/j.tws.2023.110545.

Koczubiej S., Cichon C. (2014). "Global static and stability analysis of thin-walled structures with open cross-sections using FE shell-beam models," *Thin-Walled Structures* 82, 196-211.

Latif, W., White, D.W. (2021). "Flange local post-buckling resistance and local-global buckling interaction in slender-flange welded I-section beams," *Engineering Journal*, AISC, 2nd quarter, 113-133.

MacPhedran I.J., Grondin G.Y. (2009). *Frame Stability Considering Member Interaction and Compatibility of Warping Deformations*, Structural Engineering Report No. 283, University of Alberta, Alberta, B.C.

Shayan S., Rasmussen K.J.R. (2014). "A model for warping transmission through joints of steel frames," *Thin-Walled Structures*, 82, 1-12, doi:10.1016/j.tws.2014.03.017.

Slein, R., Kamath, A.M., Latif, W., Phillips, M.L., Sherman, R.J., Scott, D.W., White, D.W. (2022). *Enhanced Characterization of the Flexural Resistance of Built-Up I-Section Members,"* Report No. 22-03, School of Civil and Environmental Engineering, Georgia Institute of Technology, Atlanta, GA.

Slein, R.,, Kamath, A.M., Phillips, M., Sherman, R.J., Scott, D.W., White, D.W. (2023). "Experimental and analytical assessment of the LTB resistance of built-up steel I-section members," *Journal of Constructional Steel Research*, doi/10.1016/j.jcsr.2022.107771.

Szalai J. (2010). "Use of eigenvalue analysis for different levels of stability design" *Stability and Ductility of Steel Structures*, SDSS, Rio de Janeiro, Brazil.

Szalai, J. (2011a). "The 'General Method' of EN 1993-1-1," *NSC*, April. 30-31.

Szalai, J. (2011b). "Practical application of the 'general method' of EN 1993-1-1," *NSC*, May, 30-32.

Szalai, J. (2017). "Complete generalization of the Ayrton-Perry formula for beam-column buckling problems" Engineering Structures 153, 205-223.

Szalai J, Papp F. (2010) "On the theoretical background of the generalization of Ayrton-Perry type resistance formulas." Journal of Constructional Steel Research 66, 670–679.

Szalai J, Papp F. (2011). "Theory and application of the general method of Eurocode 3 Part 1–1." In: Dunai L, editor. 6th European conference on steel and composite structures. Budapest, Hungary

Vaszilievits-Sömjén, B., Szalai, J. (2018). "Simple superelement model of warping transfer in moment connections between I-sections," *Ninth International Conference on Advances in Steel Structures (ICASS2018)*, Hong Kong, China, doi/10.18057/ICASS2018.P.036.

Vaszilievits-Sömjén, B., Szalai, J., Rad, M.M. (2019). "Validation of simple superelement model of warping transfer in moment connections of portal frames." *ce/papers*, 3: 373-378. doi.org/10.1002/cepa.1069.

White, D.W., Jeong, W.Y., Slein, R. (2021). *Frame Design Using Nonprismatic Members,"* Design Guide 25, 2nd Ed., American Institute of Steel Construction, Chicago, IL.

White, D.W., Jeong, W.Y, Slein, R. (2022). "Tech Tips for Tapered Members," *Modern Steel Construction*, March.

Wu L., Mohareb M. (2013). "Finite-element formulation for the lateral torsional buckling of plane frames, *Journal of Engineering Mechanics*, 139(4), 512-524.